Enhanced fluoride adsorption on aluminum-impregnated kenaf biochar: adsorption characteristics and mechanism

Moon-Yeong Choi
Hankyong National University
Chang-Gu Lee
Hankyong National University
Seong-Jik Park (parkseongjik@hknu.ac.kr)
Hankyong National University https://orcid.org/0000-0003-2122-5498

Research Article

Keywords: kenaf, biochar, fluoride removal, impregnation, Al-based adsorbent

Posted Date: April 19th, 2022

DOI: https://doi.org/10.21203/rs.3.rs-1504419/v1

Enhanced fluoride adsorption on aluminum-impregnated kenaf biochar: adsorption characteristics and mechanism

Moon-Yeong Choi [a], Chang-Gu Lee [b], Seong-Jik Park [a,*]

[a] *Department of Bioresources and Rural System Engineering, Hankyong National University, Anseong 17579, Republic of Korea*

[b] *Department of Environmental and Safety Engineering, Ajou University, Suwon 16499, Republic of Korea*

∗ Corresponding author: S.-J. Park (E-mail address: parkseongjik@hknu.ac.kr; Fax: +82-31-670-5139; ORCID: 0000-0003-2122-5498)

Statements and Declarations

Conflicts of interest: The authors declare that they have no competing interests.

Authors' contributions

Moon-Yeong Choi: Writing-original draft, Experiment, Data analysis; **Chang-Gu Lee:** Writing-review and editing; **Seong-Jik Park:** Conceptualization, Writing-review & editing, Supervision, Funding acquisition

Funding: This work was supported by the Cooperative Research Program for Agriculture Science and Technology Development (Project No. PJ01477903) of the Rural Development Administration, Republic of Korea.

Ethics approval and consent to participate: Not applicable

Consent for publication: Not applicable

Consent for participation: Not applicable

Availability of data and materials

All data generated or analyzed during this study are included in this published article.

The datasets used and/or analyzed during the current study are available from the corresponding author on reasonable request.

Abstract

The fast-growing plant kenaf was pyrolyzed to biochar, and the biochar was impregnated with aluminum to improve its fluoride adsorption capacity. The Al-impregnated kenaf biochar (Al-KNF-BC) was pyrolyzed at different temperatures (300–700 °C). The specimen treated at 300 °C (Al-KNF-300) showed the highest fluoride adsorption capacity. The kinetics and equilibrium adsorption of fluoride by Al-KNF-300 followed the pseudo-second-order and Langmuir models, respectively. According to the Langmuir model, the maximum fluoride adsorption capacity of Al-KNF-300 is 13.93 mg/g. The enthalpy and entropy of fluoride adsorption by Al-KNF-300 were 37.80 kJ/mol and 124.1 J/mol·K, respectively. Fluoride adsorption by Al-KNF-300 was favorable at pH values as low as pH 3, and the effect of anion competition followed the order $HCO_3^- > SO_4^{2-} > NO_3^- > Cl^-$. In experiments with different adsorbent dose, the maximum adsorption efficiency of 99.23% was obtained at an adsorbent concentration of 16.67 g/L, at which the fluoride concentration decreased from 100 mg/L to <1.5 mg/L (the drinking water standard). Al-KNF-300 is an effective and inexpensive adsorbent for removing fluoride from contaminated water to meet drinking water standards.

Keywords: kenaf, biochar, fluoride removal, impregnation, Al-based adsorbent

1 Introduction

Fluoride occurs naturally and is released from rocks into water, air, and soil; it is naturally present in groundwater, freshwater, chlorine sources, and rainwater in urban areas. Fluoride is used in many dental products to strengthen tooth enamel and prevent cavities. Studies have shown that fluoride can be added to drinking water at low concentrations to reduce the incidence of tooth decay in local populations, and many developed countries fluoridate their tap water (Podgorny and McLaren 2015; Jones et al. 2005). However, prolonged exposure to drinking water with a high fluoride concentration can have side effects such as dental and skeletal fluorosis, which can damage bones and joints. The population affected by fluorosis has increased over the past 50 years, and 260 million people worldwide are estimated to be affected by fluorosis (Amini et al. 2008). The World Health Organization guideline for the fluoride content at which drinking water becomes unhealthy is 1.5 mg/L (World Health Organization 2017). Additionally, according to the US Environmental Protection Agency (EPA), the maximum contaminant level of fluoride in public water systems is 4 mg/L; the secondary maximum contaminant level is 2 mg/L, which requires special notice to the EPA (US Environmental Protection Agency 2020). Fluoride concentrations of 0.01–3 mg/L in freshwater and 1–35 mg/L in groundwater have been observed in some natural water systems (Tripathy et al. 2006). Because excess fluoride is harmful to humans, safe treatment of contaminated water is needed to make the water drinkable.

Methods commonly used for the defluorination of water include adsorption (Chen et al. 2010; Çengeloğlu et al. 2002; Turner et al. 2005), precipitation (Turner et al. 2005; Chang and Li 2007), ion exchange (Samadi et al. 2014), electrodialysis (Amor et al. 2001), and membrane filtration (Elazhar et al. 2009). Adsorption is the most commonly used method because it is cost-effective, easy to apply, and able to remove fluoride even at low concentrations. The

performance of the adsorption system depends on the characteristics of the adsorbent, and in recent decades, various adsorbents have been developed for the removal of fluoride from drinking water. Many materials have been tested, such as activated aluminum oxide (Tang et al. 2009a; Ahamad et al. 2018; Ghorai and Pant 2004), amorphous aluminum oxide (Li et al. 2001), Al-modified biochar (Meilani et al. 2021), an Fe- and Ca-based adsorbent (Biswas et al. 2007), clam shell (Lee et al. 2021b; Choi et al. 2021), egg shell (Lee et al. 2021a), clay (Karthikeyan et al. 2005; Chen et al. 2011), bone charcoal (Leyva-Ramos et al. 2010; Medellin-Castillo et al. 2007), metal oxides (Dhillon et al. 2017), and zeolites (Sun et al. 2011). As fluoride forms strong bonds with Al and Ca, Al- and Ca-based adsorbents are generally used for fluoride removal. Ca-based adsorbents have a low fluoride reduction limit (>2 mg/L) and are not suitable for drinking water treatment (Wang and Reardon 2001; Fan et al. 2003). By contrast, Al compounds have a strong affinity for fluoride; they are porous materials with high fluoride adsorption capacity and can lower the fluoride concentration to 2 mg/L (Farrah et al. 1987; Tchomgui-Kamga et al. 2010). The surface of aluminum oxide is lipophilic and positively charged, and pore structure is easily formed by process control (Zhou et al. 2021). Activated alumina can also remove other toxic elements in groundwater such as arsenic and selenium (Farooqi et al. 2007; Tang et al. 2009a). Al-based materials can be used as fluoride adsorbents; however, aluminum oxide is expensive, and its optimal pH for fluoride adsorption is in the acidic range, limiting its practical application in drinking water (Li et al. 2001). Therefore, it is desirable to fabricate an Al-based adsorbent material that is cheaper and more environmentally friendly, but equally effective in removing fluoride from drinking water.

Methods of manufacturing Al-based adsorbents for improving fluoride removal include doping (Rojas-Mayorga et al. 2015) and loading (Fan et al. 2021) on carbon-based materials such as biochar. Biochar is obtained by pyrolyzing biomass in an anoxic environment; it is rich

in carbon, inexpensive, stable, and environmentally friendly (Ahmed et al. 2016). Previous studies have shown that the chemical structure, surface roughness, and specific surface area of biochar are affected by the biomass pyrolysis conditions (Mohan et al. 2014; Zhou et al. 2021). Biochar obtained under the optimal pyrolysis conditions can be a suitable adsorbent material. However, its fluoride adsorption is limited, and it requires modification (Meilani et al. 2021). Because biochar has a complex pore structure and abundant functional groups, it can be loaded with Al, which has a strong affinity for fluoride (Mian and Liu 2018).

In this study, kenaf biochar is used as an adsorbent. Kenaf (*Hibiscus cannabinus*) is an annual grass with a short growth cycle that belongs to the family *Malvaceae*. It can grow to more than 3 m in 3 months under varying weather conditions and moderate ambient conditions (with small amounts of pesticides and herbicides) (Azwa and Yousif 2013; Sellers 1999; Nishino et al. 2003). Kenaf fibers are composed of cellulosic hemicellulose and lignin; cellulosic material, which is known to be an effective adsorbent, makes up approximately 47% of the plants (Malik et al. 2017). In addition, studies have shown that both the outer shell and inner core of kenaf stems contain fibrous components, which enhance adsorption (Shamsuddin et al. 2016). Thus, the high productivity and adsorption potential of kenaf make it a suitable biomass material for use as an adsorbent. Kenaf has been used to remove various contaminants such as dyes (Mahmoud et al. 2012), Cu (Hasfalina et al. 2012), Cr (Borna et al. 2016), rare earth elements (Rahman et al. 2017), Ni (Hasfalina et al. 2010), triclosan (Cho et al. 2021), and fluoride (Yusof et al. 2015) from aqueous solutions. In a previous study, fluoride adsorption using kenaf modified with *N*-trimethylammonium yielded a maximum adsorption capacity of 13.98 mg/g (Yusof et al. 2015). However, the chemical used for modification is expensive, and the fluoride reduction limit is 2 mg/L or more, making it unsuitable for drinking water treatment.

131 Therefore, in this study, an Al-biochar complex was prepared by Al impregnation and
132 thermal decomposition of kenaf to improve the fluorine adsorption capacity. Al-impregnated
133 kenaf biochar (Al-KNF-BC) was prepared at various pyrolysis temperatures, and the fluoride
134 adsorption capacity of the samples was compared. In addition, the fluoride adsorption
135 mechanism of Al-KNF-BC was physically and chemically analyzed using field emission
136 scanning electron microscopy (FE-SEM), Brunauer–Emmett–Teller (BET) analysis,
137 thermogravimetric analysis/differential thermal analysis (TGA/DTA), X-ray diffraction (XRD)
138 analysis, and Fourier-transform infrared (FTIR) spectroscopy. The adsorption mechanism of
139 the Al-KNF-BC sample with the highest fluoride adsorption capacity was analyzed using
140 kinetics, equilibrium, and thermodynamic adsorption experiments and model analysis. In
141 addition, the effects of pH, the presence of competing anions, and adsorbent dose on fluoride
142 adsorption were investigated.
143
144 **2. Materials and Methods**
145 **2.1 Production of Al-impregnated kenaf biochar**
146 The kenaf used as the base material for Al impregnation was procured from the Agricultural
147 Research Institute (Jeonbuk, Korea). The chemical composition and physical properties of
148 kenaf are available in the literature (Kim and Um 2020; Cho et al. 2021). Only the stem of the
149 kenaf was used, not the leaves and roots; the stem was ground and then sieved to 425 μm. It
150 was washed with deionized water to completely remove impurities and dried in an oven at
151 80 ℃ for 24 h.
152 Al impregnation was performed with reference to the optimal Al content determined by the
153 response surface methodology in a previous study (Meilania et al. 2021). To impregnate the
154 kenaf with a surface $Al(OH)_3$ layer before thermal decomposition, 500 mL of a 0.741 M (5.89%)

aluminum chloride ($AlCl_3$, Sigma-Aldrich, USA) solution was first placed in a stirred reactor. Next, 50 g of dry kenaf was added and thoroughly soaked. The mixture was neutralized to pH 7 by the addition of a 10 M NaOH (Samchun, Korea) solution with stirring at 150 rpm. Under these conditions, the kenaf surface in the mixture is modified by a strong chelation reaction with Al, and the adsorbed Al^{3+} is present mainly in the form of $Al(OH)_3$ at pH 7 (Mahfoudhi and Boufi 2020). The mixture was stirred for 4 h to prepare a homogeneous slurry. The slurry was dried in an oven at 110 °C to obtain Al-impregnated kenaf (Al-KNF).

To pyrolyze the Al-KNF, a sample was injected into a stainless steel tube (L/D: 55/5.5 cm), which was heat-treated in a muffle furnace (CRFT 830S, Dongseo Science Co., Ltd., Korea) at 300, 400, 500, 600, or 700 °C for 1 h. To maintain anoxic conditions, which are required for pyrolysis, an inert gas (N_2 gas, >99.9%) was injected at a flow rate of 0.5 L/min to purge the inside of the tube, and the heating rate was 20 °C/min. The Al-KNF-BC samples pyrolyzed at each temperature are denoted as follows: Al-KNF-300, Al-KNF-400, Al-KNF-500, Al-KNF-600, and Al-KNF-700.

Fluoride adsorption by the Al-KNF-BCs prepared at various pyrolysis temperatures was compared. A 1000 mg/L fluoride solution was prepared by dissolving 2.2101 g of sodium fluoride (NaF, Sigma-Aldrich, USA) in 1 L of deionized water and then diluted five times to 200 mg/L. All materials were weighed using an analytical electronic balance with a reproducibility of 0.1 mg. Al-KNF (0.1 g) was placed a 50 mL conical tube, and 30 mL of a 200 mg/L fluoride solution was injected with a pipette. The conical tube was placed in an incubator and stirred at 25 °C and 100 rpm for 12 h for the reaction. The reacted mixture was first filtered using a qualitative filter paper (No. 2, Advantec, Japan) with a pore size of 5 μm. It was then filtered using a syringe filter (Advantec, Japan) with a pore size of 0.45 μm. The

fluoride in the filtered solution was adsorbed using ion chromatography (DX-120, Dionex, USA), and the residual fluoride concentration was measured.

2.2 Adsorption characterization

Several characterization methods were used to determine the chemical composition, morphology, and fluoride adsorption reaction mechanism of Al-KNF-NT (not treated) and pyrolyzed Al-KNF-BC samples. All samples were washed with deionized water and dried before FE-SEM and XRD measurements. The surface morphology of the samples was observed by FE-SEM (S-4700, Hitachi, Japan). Energy-dispersive X-ray spectroscopy (EDS) was performed using an instrument attached to the scanning electron microscope to investigate the elemental composition. The specific surface area of Al-KNF was calculated using the BET equation and observations of the adsorption/desorption of N_2 gas. TGA was performed using a thermogravimetric analyzer (Pyris 1, PerkinElmer, USA) at 30–700 °C with a heating rate of 10 °C/min in N_2 gas. The crystal structure of the samples was determined by XRD analysis (SmartLab, Rigaku, Japan). Functional groups on the biochar surface were identified by FTIR spectroscopy (Nicolet 6700, Thermo Fisher Scientific, UK).

2.3 Data analysis

The amount of fluoride adsorbed per unit mass of adsorbent was calculated using the mass balance equation:

$$q_e = \frac{(C_i - C_e) \times V}{m} \quad (1)$$

where C_i (mg/L) is the initial fluoride concentration, C_e (mg/L) is the residual fluoride concentration at equilibrium, V (L) is the solution volume, and m (g) is the adsorbent dose.

The fluoride adsorption efficiency (%) of the adsorbent was calculated as follows:

$$\text{Adsorption efficiency } (\%) = \frac{(C_i - C_e)}{C_i} \times 100 \quad (2)$$

201 The mathematical expressions (nonlinear fits) of the pseudo-first-order (PFO) and pseudo-
202 second-order (PSO) kinetic models are shown in Eqs. (3) and (4), respectively (Lagergren 1898;
203 Ho and Mckay 1998).

$$q_t = q_e(1 - e^{-k_1 t}) \quad (3)$$

$$q_t = \frac{k_2 q_e^2 t}{1 + k_2 q_e t} \quad (4)$$

204 where q_t (mg/g) and q_e (mg/g) are the amounts of fluoride adsorbed at time t (h) and equilibrium,
205 respectively, and k_1 (h^{-1}) and k_2 (g/mg·h) are the PFO and PSO adsorption rate constants,
206 respectively.

207 The nonlinear mathematical expressions of the Langmuir and Freundlich isotherm models
208 are shown in Eqs. (5) and (6), respectively (Langmuir 1916; Freundlich 1907).

$$q_e = \frac{Q_{max} K_L C_e}{1 + K_L C_e} \quad (5)$$

$$q_e = K_F C_e^{\frac{1}{n}} \quad (6)$$

209 where Q_{max} (mg/g) and K_L (L/mg) are the maximum adsorption capacity of the adsorbent and
210 the Langmuir constant related to the adsorption energy of the adsorbent, respectively. K_F (mg/g
211 $(mg/L)^{-1/n}$) and n (-) are the Freundlich constant and adsorption strength, respectively.

212 The thermodynamic parameters were calculated as follows:

$$\Delta G^0 = -RT \ \ln(K_e) \quad (7)$$

$$\ln(K_e) = \frac{\Delta S^0}{R} - \frac{\Delta H^0}{RT} \quad (8)$$

$$K_e = \frac{aq_e}{C_e} \quad (9)$$

where ΔG^0 (kJ/mol), ΔS^0 (J/mol·K), and ΔH^0 (kJ/mol) are the changes in the standard Gibbs free energy, enthalpy, and entropy, respectively; a (g/L) is the adsorbent dose; q_e (mg/g) is the maximum adsorption amount; T (K) is the absolute temperature; and R (=8.314 J/mol·K) is the universal gas constant.

2.4 Adsorption experiments

Fluoride adsorption experiments were conducted to examine the kinetics, equilibrium, and thermodynamics and the effects of pH, ion competition, and adsorbent dose. In all experiments, the adsorbent was Al-KNF-300, which had the highest adsorption capacity per unit mass in the previous experiment. In addition, unless otherwise specified, in all experiments, 0.1 g of adsorbent and 30 mL of 100 mg/L fluoride solution were reacted in a 50 mL conical tube, and the conical tube was shaken for 12 h at 100 rpm in an incubator at 25 °C. In the kinetic experiment, a 100 mg/L fluoride solution was injected, and the reaction time (0.25–72 h) was varied at a constant temperature (25 °C). In the equilibrium isotherm experiment, the concentration of the initial fluoride solution (5–150 mg/L) was varied at a constant temperature (25 °C), and the reaction was conducted for 12 h. In the thermodynamic experiment, the reaction temperature was varied (15, 25, and 35 °C), and the reaction was performed in a 100 mg/L fluoride solution for 12 h. The adsorption experiment using fluoride solutions of different pH was performed after the pH of the 100 mg/L fluoride solution was adjusted to 3, 5, 7, 9, and 11 using 0.1 M NaOH and 0.1 M HCl solutions. Fluoride adsorption experiments with different competing anions were performed using 1 mM and 10 mM $NaHCO_3$, Na_2SO_4, NaCl, and $NaNO_3$ in a 100 mg/L fluoride solution. Reagents (HCl, NaOH, $NaHCO_3$, Na_2SO_4, NaCl, and $NaNO_3$) of reagent grade were purchased from Samchum (Korea). In the adsorption experiment

on the effects of adsorbent dose, 3.33, 6.67, 10, 13.33, and 16.67 g/L of the adsorbent was injected to react with the fixed volume (30 mL) of 100 mg/L fluoride solution.

3. Results and Discussion

3.1 Characteristics of Al-KNF

Fig. 1 shows the amount of fluoride adsorbed by the untreated and biochar samples (Al-KNF-NT and Al-KNF-BC, respectively). The amount of fluoride adsorbed per unit mass of Al-KNF increased sharply to 13.72 mg/g for the sample pyrolyzed at 300 °C, which is approximately 9.6 times that of Al-KNF-NT (1.43 mg/g). At pyrolysis temperatures above 400 °C, the amount of fluoride adsorbed decreased and did not differ significantly from that of Al-KNF-NT. To determine why Al-KNF-300 showed the highest fluoride adsorption and investigate the adsorption mechanism, physical and chemical analyses of Al-KNF were performed.

The surface morphology and physical properties of Al-KNF were observed using FE-SEM and BET analysis, as shown in Fig. S1 and Table 1. The surface of Al-KNF has a thin porous structure unique to biochar and becomes rough with increasing pyrolysis temperature. The reason is that pores and cracks are formed on the biochar surface as volatiles are generated and escape during heat treatment, increasing the porosity of the structure (Abdel-Fattah et al. 2015). The surfaces of Al-KNF-NT and Al-KNF-300 contain no crystal-like material, possibly because of the presence of amorphous aluminum. However, material that is assumed to be nano- and microsize Al particles (Al_2O_3) is distributed on the surface of the Al-KNF-BCs pyrolyzed at 400–700 °C, which was confirmed by the XRD results (Mahfoudhi and Boufi 2020; Sun et al. 2008).

The BET specific surface area of Al-KNF-NT was not measured because the pores of Al-KNF were blocked by the $AlCl_3$ and NaOH used for impregnation. The BET results show that the clogged pores of Al-KNF-NT cannot adsorb fluoride; consequently, less fluoride is adsorbed compared to the other adsorbents. The specific surface area of the Al-KNF-BCs increased from 27.24 to 79.29 m^2/g as the pyrolysis temperature increased from 300 to 700 °C, and the pore volume and pore size increased with increasing specific surface area. The reason is that the cracking of cellulose, hemicellulose, and lignin with oxidation depends on pyrolysis temperature; thus, more micropores are created and the internal surface area increases with increasing temperature (Zhuang 2021). Because the observed pore size of the Al-KNF-BCs is 4–22 nm, which is much larger than the radius of the fluoride atom (1.33 Å), F^- may be dispersed into the inner layer of Al-KNF. However, these physical changes (surface roughness and specific surface area), which might increase the adsorption potential of Al-KNF, cannot fully explain the high fluoride adsorption of Al-KNF-300.

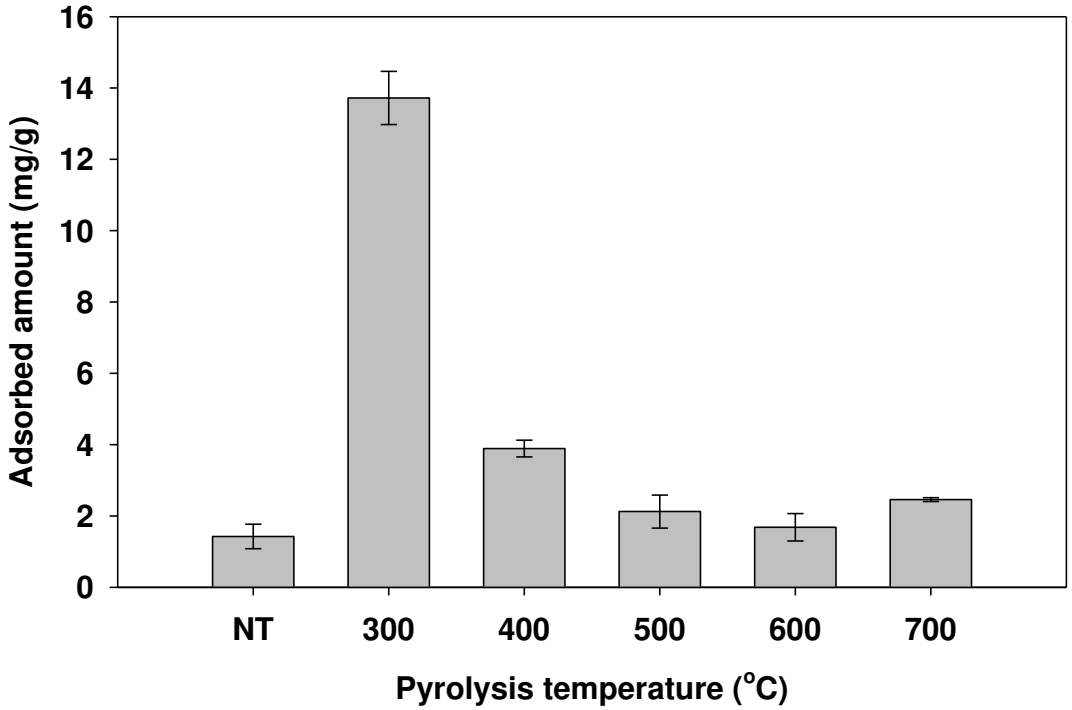

Fig. 1. Fluoride adsorption capacity of Al-KNF obtained at various pyrolysis temperatures (initial F concentration: 100 mg/L, adsorbent dose: 3.33 g/L, reaction temperature: 25 °C, time: 12 h)

Table 1. Elemental composition and physical properties of Al-KNF

Temperature (°C)	Elemental composition[a]						Physical properties[b]		
	C %	O %	Na %	Al %	Cl %	O/C	Specific surface area (m^2/g)	Pore volume (cm^3/g)	Pore size (nm)
Not treated	21.9	35.8	0.2	29.1	12.9	1.6	-	-	-
300	58.3	31.2	1.5	6.0	3.0	0.5	27.24	0.031	4.62
400	61.7	26.0	1.9	6.6	3.8	0.4	72.73	0.072	3.94
500	65.1	22.0	1.2	8.2	3.5	0.3	67.28	0.082	4.89
600	60.0	24.1	1.0	11.8	2.6	0.4	79.11	0.101	5.11

700	42.6	26.4	1.8	25.8	3.4	0.6	79.29	0.102	5.16

[a] Obtained by EDS

[b] Obtained by BET method

TGA/DTA revealed a decrease of 15.5% in the total weight of Al-KNF at temperatures of 30–700 °C, as shown in Fig. 2. Approximately 4.5% of the weight loss is attributed to moisture loss, because the weight loss up to 200 °C is due to the evaporation of adsorbed water on the material surface. The sharp peak in the DTA curve from 200 to 420 °C is represented by two curves. The highest peak in the DTA curve appears at 370.2 °C. The overall weight loss (7.6%) up to 200–420 °C may be due to the decomposition of cellulose and hemicellulose in kenaf (Ferrara et al. 2014). Here, the sharp weight loss up to 240–300 °C may result from the removal of surface functional groups and hydroxyl groups generated by co-precipitation (Ding et al. 2018; Ebadi et al. 2021). The moderate weight loss at 420–700 °C may be due to loss of C, that is, the continuous breakdown of lignin (Cho et al. 2021).

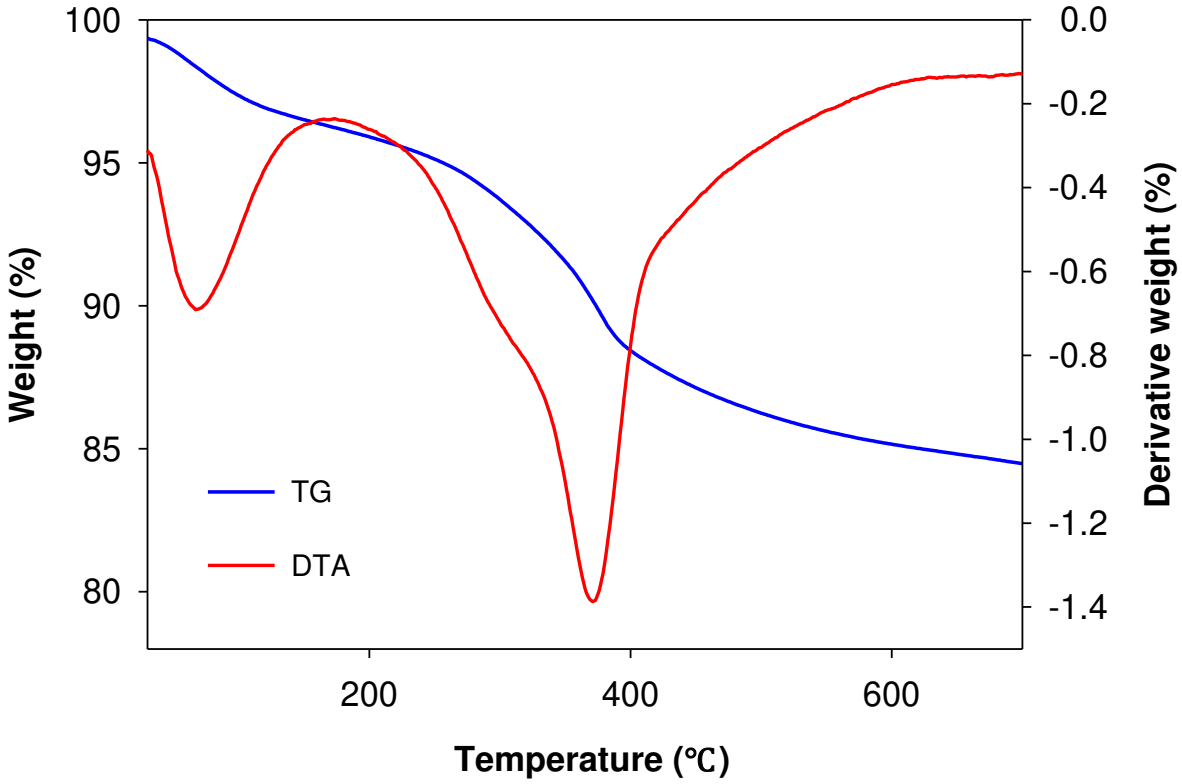

292

293 **Fig. 2.** Thermogravimetric (TG) weight and differential thermal analysis (DTA) of Al-KNF in
294 the temperature range of 30-700 ℃

295

296 Table 1 shows the results of elemental analysis of Al-KNF using EDS. Al-KNF is composed
297 mainly of C, O, Na, Al, and Cl. Here, Na and Cl may indicate the presence of NaCl produced
298 during Al impregnation and not removed by washing. According to Table 1, Al-KNF-NT has a
299 Cl content of 12.9%, which was not easily removed by washing. Chlorine remaining on the
300 surface of Al-KNF-NT may compete with fluoride and interfere with fluoride adsorption on
301 the adsorbent surface. This fact may explain why Al-KNF-NT adsorbed less fluoride than Al-
302 KNF-300 despite the high Al content. In addition, as the pyrolysis temperature of Al-KNF-BC
303 increases (>500 ℃), the C content decreases and the Al content increases. The decrease in C
304 content is attributed to the combustion of organic matter with increasing carbonization

temperature, and a slight decrease in the C content simultaneously causes a high mineral content (Stefaniuk et al. 2015). The O/C ratio of Al-KNF decreased during heat treatment, indicating increased hydrophobicity and fewer polar groups (Zhang et al. 2011).

The XRD patterns of Al-KNF indicate the crystallinity of the samples (Fig. 3). The reflection peaks are identified as NaCl, AlOOH, and Al_2O_3 (JCPDS card numbers 05-0628, 84-0175, and 80-0955, respectively). These minerals are present because $AlCl_3$ was used to impregnate the kenaf surface with Al, and this result is consistent with the EDS data. The line broadening of the XRD patterns of the prepared sample indicates small particle size or amorphous boehmite structure (Sun et al. 2008). As the pyrolysis temperature increases, the Al peak becomes sharper because of the crystallization of Al. In addition, in the Al-KNF-BCs treated at ≥400 °C, Al is present in the form of aluminum oxide rather than aluminum hydroxide because of dehydration, which is consistent with the results of other studies (Sun et al. 2008; Zhang et al. 2019). Amorphous Al is more effective at adsorbing fluoride because the dissolution of Al is more pronounced in the amorphous phase than in the crystalline phase (Harrington et al. 2003). In addition, the amorphous form of aluminum hydroxide exhibits better defluorination performance than aluminum oxide, probably owing to the presence of hydroxyl groups, which supply abundant electrons (Chen et al. 2022). Consequently, Al-KNF-300 (which contains aluminum hydroxide) adsorbs more fluoride than the specimens pyrolyzed at ≥400 °C (which contain aluminum oxide) in this experiment.

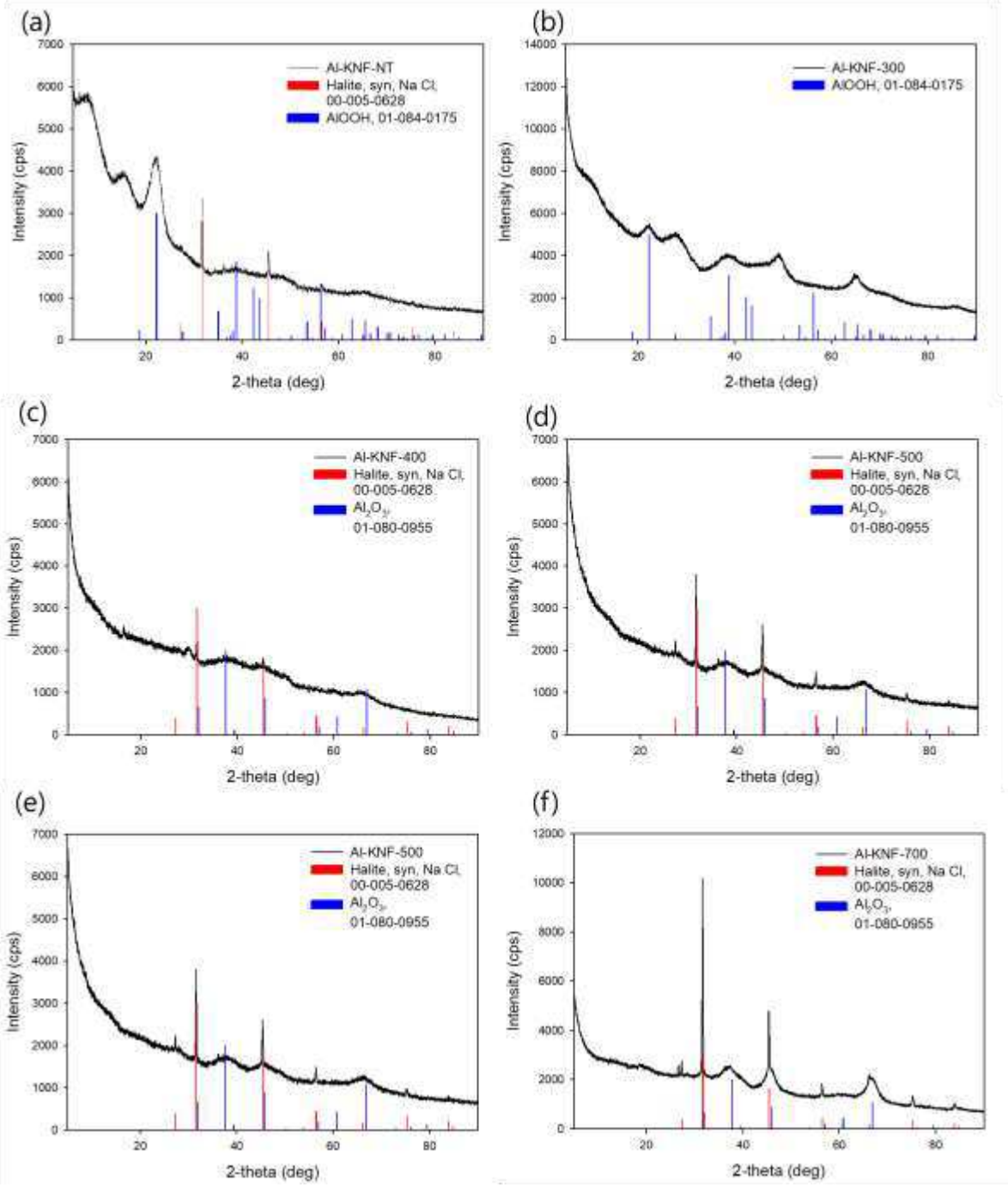

Fig. 3. XRD patterns of Al-KNF: (a) Al-KNF-NT, (b) Al-KNF-300, (c) Al-KNF-400, (d) Al-KNF-500, (e) Al-KNF-600, and (f) Al-KNF-700

Fig. S2 shows the FTIR spectra of Al-KNF-NT and the Al-KNF-BCs pyrolyzed at each temperature. The broad band centered at 3300–3400 cm^{-1} can be attributed to the stretching vibration of the OH group, and the libration band derived from the OH^- group is clearly visible at 660 cm^{-1} (Rapacz-Kmita et al. 2005). The peak near 2140–2100 cm^{-1} indicates weak triple-bond stretching of C and C. The 1602 cm^{-1} peak is due to aromatic ring stretching oscillations (C=C and C=O), indicating the formation of carbonyl-containing groups and initial aromatization of the precursor (Guo and Rockstaw 2006; Liu et al. 2015). This peak was most intense at a thermal decomposition temperature of 300 °C and tended to decrease as the thermal decomposition temperature increased. This result indicates that the carboxyl groups are decomposed at high temperature, and the aromatization of the activation mixture increases (Guo and Rockstaw 2006). The peaks of Al-KNF-400 and Al-KNF-500 at 1165–1252 cm^{-1} are attributed to C–O stretching oscillations and indicate that the samples contain organic substances such as carboxylic acids and alcohol anhydrides (Lin et al. 2009). At higher pyrolysis temperatures (600 and 700 °C), the broad OH band at 3300–3400 cm^{-1} and C–O stretching oscillations at 1165–1252 cm^{-1} decreased and ultimately disappeared. The adsorption band in the range of 500–800 cm^{-1} from Al-KNF-NT to Al-KNF-400 is characteristic of the Al–O–H band (Jagtap et al. 2011). However, the Al-KNF-BCs heated above 500 °C showed only the Al–O–Al adsorption band, indicating the complete transformation of AlOOH to Al_2O_3 because of dehydration (Zhang et al. 2019).

Al-KNF-300 adsorbed more fluoride than Al-KNF-NT because pyrolysis created pores and Cl^- was washed out after pyrolysis. In comparison with the other Al-KNF-BCs, Al-KNF-300 had lower surface roughness and a smaller specific surface area; no significant difference in Cl content was found. Therefore, the adsorption mechanism of Al-KNF-300 cannot be interpreted solely in terms of these physical changes and Cl content. At pyrolysis temperatures

above 400 °C, the Al peak became sharper because of Al crystallization, and the Al on the surface of the Al-KNF-BCs was changed from AlOOH to Al_2O_3. FTIR analysis confirms that the Al–O–H band of the Al-KNF-BCs disappeared when the pyrolysis temperature exceeded 500 °C, indicating the removal of the hydroxyl group at high pyrolysis temperatures. Aluminum hydroxide has more hydroxyl groups than aluminum oxide and thus is advantageous for adsorption, and amorphous Al has better solubility than crystalline Al. Consequently, the adsorption performance of Al-KNF-300, which is more amorphous and has Al in the form of aluminum hydroxide on the surface, is superior to that of the other Al-KNF-BCs.

3.2 Kinetic adsorption by Al-KNF-300

The kinetic adsorption of fluoride by Al-KNF-300 was performed at a constant reaction temperature (25 °C) for various reaction times (0.25–72 h). The standard deviation of the experimental results was ±2%. Fluoride adsorption increases rapidly from 2.46 to 10.52 mg/g at the beginning of the process (0.25–6 h). Subsequently, the adsorption rate decreases until it approaches equilibrium at 12 h (12.85 mg/g). The adsorption then increases slightly (by <1 mg/g) to 13.74 mg/g at 72 h. Therefore, a fluoride adsorption equilibrium time of 12 h was used in further adsorption experiments. Here, fluoride adsorption requires a concentration gradient between the solution and adsorbent. Initially, many sorption sites are available, and thus the adsorption rate is high. Later in the process, the adsorption site availability and concentration gradient decrease, and the adsorption rate also decreases (Ramos-Vargas et al. 2018).

Nonlinear regression analysis using the PFO and PSO models was applied to the results of the kinetics experiments using the parameter values listed in Table S1. Because the PSO model has a higher correlation coefficient (R^2 = 0.992), it can be said to explain the experimental data

379 better. In addition, the equilibrium adsorption value (q_e; mg/g) obtained using the PSO model
380 exactly matches the equilibrium value of the experimental data (13.73 mg/g). Therefore, it can
381 be concluded that the PSO model is preferable to the PFO model for explaining fluoride
382 adsorption by Al-KNF-300. This result suggests that the adsorption rate is controlled by either
383 electron exchange between the adsorbent and solution or chemical adsorption related to the
384 valence force due to shared anions (Wang et al. 2018; Mayakaduwa et al. 2016; Feng et al.
385 2011).
386

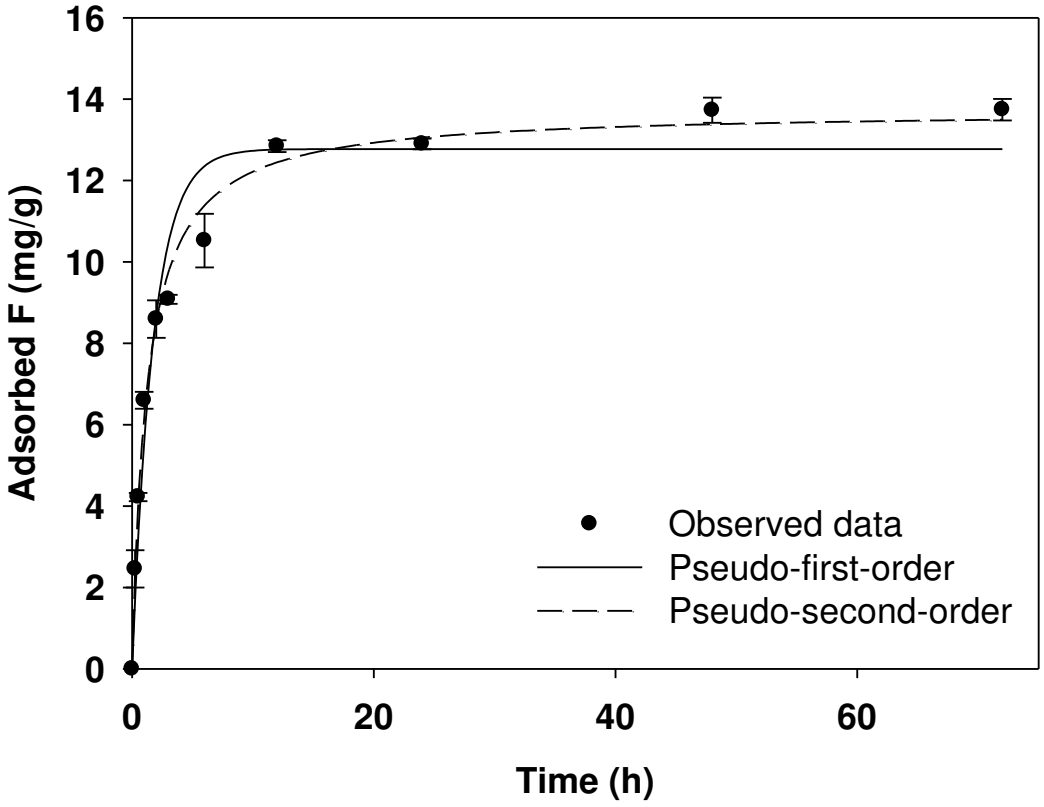

387

388 **Fig. 4.** Results of kinetics experiment on Al-KNF-300 and nonlinear regression analysis of
389 PFO and PSO models (initial F concentration: 100 mg/L, adsorbent dose: 3.33 g/L, reaction
390 temperature: 25 °C, time: 0.25, 0.5, 1, 2, 3, 6, 12, 24, 48, and 72 h)
391

3.3 Equilibrium isotherm of Al-KNF-300

An equilibrium adsorption experiment using Al-KNF-300 was performed at a constant temperature (25 °C) with various initial concentrations (5–150 mg/L). Fig. S3 shows the relationship between the adsorption amount and residual concentration after adsorption. When the initial fluoride concentration was low (5–30 mg/L), more than 95% of the fluoride was removed, indicating that the fluoride concentration of most fluoride-contaminated groundwater (1–35 mg/L) can be reduced to below the drinking water limit (<1.5 mg/L) (Tripathy et al. 2006; World Health Organization 2017). However, as the fluoride concentration increased, the residual concentration increased, and the adsorption amount reached equilibrium. This equilibrium occurs because F^- occupies all of the surface active sites (Chen et al. 2016; Tchomgui-Kamga et al. 2010). In the experiment, equilibrium was first reached at an initial fluoride concentration of 100 mg/L, and 14.22 mg/g of fluoride was adsorbed at the highest fluoride concentration of 150 mg/L. Because Al-KNF-300 can remove fluoride to some extent even at high fluoride concentrations, all batch tests except for the equilibrium test were performed at an initial fluoride concentration of 100 mg/L.

Equilibrium isotherm analysis of adsorption equilibrium data can reveal the adsorption capacity, which is very important in the design of adsorption systems (Iriel et al. 2018). The results of this equilibrium experiment were modeled using equilibrium isotherm models (the Langmuir and Freundlich models) and the parameter values listed in Table S2. The correlation coefficient (R^2) values show that the Langmuir model fits the data for fluoride adsorption by Al-KNF-300 much better than the Freundlich model. Therefore, it can be inferred that the adsorbate molecules do not interact, and adsorption occurs in a monolayer on a homogeneous surface (Salifu et al. 2013). The Q_{max} value (13.93 mg/g) given by the Langmuir model of fluoride adsorption by Al-KNF-300 is similar to the equilibrium value in the experimental data

(14.22 mg/g). The fluoride adsorption capacity obtained in this study was compared with that of various natural and synthetic adsorbents (Table 2). Because direct comparison with other adsorbents is difficult, the initial fluoride concentration, particle size, pH, and temperature are presented along with the fluoride adsorption amount. The results show that Al-KNF-300 has a relatively high fluoride adsorption capacity (in the moderate to high range) compared to the other adsorbents. In addition, the particle size of the adsorbent used for fluoride removal in the literature varies from tens to thousands of micrometers, and Al-KNF-300 has a large particle size (450 μm) despite its effective fluoride adsorption ability. Adsorbents with larger particles are more accessible to filter out of aqueous solution than nano-/microsize adsorbents because they do not require further treatment for separating them from the treated water.

Table 2. Fluoride adsorption capacity of Al-KNF-300 and various other adsorbents

Adsorbent	Maximum adsorption capacity (mg/g)	Initial fluoride concentration (mg/L)	Particle size (μm)	pH	Temperature (°C)	Reference
Laterite	0.5	1–50	2000	8	-	Iriel et al. (2018)
Montmorillonite clay	1.485	-	75	-	30	Karthikeyan et al. (2005)
Kanuma mud	1.558	5–50	150	6.9	30	Chen et al. (2011)
Stilbite zeolite modified with Fe(III)	2.31	5–40	-	6.7	-	Sun et al. (2011)
Activated aluminum oxide	2.41	2.5–14	2000–5000	7	-	Ghorai and Pant (2004)

Fe–Al-impregnated granular ceramic	3.6	5–40	30–150	<6	27	Das et al. (2005)
Magnetic corn stover biochar	4.11	1–100	595–297	8	25	Mohan et al. (2014)
Waste carbon slurry	4.31	10	-	7.58	25	Gupta et al. (2007)
Corn stover biochar	6.42	1–100	595–297	8	25	Mohan et al. (2014)
Iron–tin mixed oxide	10.47	10–50	140–290	6.4 ± 0.2	25	Biswas et al. (2009)
Bone char	11.9	1–20	-	3	25	Medellin-Castillo et al. (2007)
Al-modified kenaf biochar	13.73	5–150	425	7	25	This study
N-trimethylammonium-modified kenaf	13.98	5–80	1000–2000	5.2	25	Yusof et al. (20150
Mesoporous aluminum oxide	14.26	20–250	-	6	30	Lee et al. (2010)
Protonated chitosan particles	15.87	-	-	7	30	Kusrini et al. (2015)
Quicklime	16.67	10–50	150	6.61	25 ± 2	Islam and Patel (2007)
Rare-earth-modified aluminum oxide	26.45	2–200	-	6	25	He et al. (2019)

Amorphous aluminum hydroxide hollow spheres	45.23	40–120	-	4	25.15	Zhang et al. (2016)

428

429 **3.4 Thermodynamic study of Al-KNF-300**

430 A batch test was performed at three temperatures (15, 25, and 35 ℃) to evaluate the
431 thermodynamic adsorption mechanism in terms of the effect of reaction temperature on fluoride
432 adsorption by Al-KNF-300. Using these data, the changes in the Gibbs free energy (ΔG^0),
433 enthalpy (ΔH^0), and entropy (ΔS^0) during adsorption can be calculated using the van 't Hoff
434 equation, as shown in Eq. (7). ΔH^0 and ΔS^0 were obtained as the slope and intercept,
435 respectively, in the plots of $\ln(K_e)$ versus $1/T$ in Fig. S4. The calculated thermodynamic
436 parameters are shown in Table S3. ΔG^0 decreased with increasing temperature and was negative
437 at 35 ℃. These results indicate that fluoride adsorption by Al-KNF-300 becomes more
438 spontaneous and energetically favorable with increasing system temperature (Ha et al. 2017).
439 In addition, the increase in activation energy with increasing reaction temperature suggests that
440 adsorption is an endothermic process, which is confirmed by the positive enthalpy change ΔH^0
441 (Nascimento et al. 2021). The type of interaction between the adsorbent and adsorbed substance
442 can be classified according to the magnitude of ΔH^0. In general, the interaction is controlled by
443 physical adsorption when the enthalpy change is 2–20 kJ/mol and by chemical adsorption when
444 the enthalpy change is 80–200 kJ/mol (Chaari et al. 2019; Abdilla et al. 2018; Khan et al. 2015).
445 For this experiment, ΔH^0 is 37.80 kJ/mol, which is between the physical and chemical
446 adsorption ranges, suggesting that both physical and chemical adsorption may occur in the
447 adsorption system (Shahmoradi et al. 2020; Mirsoleimani-azizi et al. 2018). The entropy
448 change (ΔS^0) is 124.41 J/kmol. The positive result indicates an increase in disorder at the

449 solid/liquid interface, which suggests that adsorption is irreversible and stable (Kasperiski et
450 al. 2018; Thue et al. 2016; Meilani et al. 2021).
451
452 **3.5 Effect of solution chemistry on fluoride adsorption by Al-KNF-300**
453 The solution pH significantly affects the degree of adsorption of fluoride because it controls
454 the interaction at the adsorbent/water interface. Low pH is desirable as the adsorption of anions
455 such as fluoride is associated with the release of OH^- from the adsorbent surface (Cengeloglu
456 et al. 2006). Al-KNF-300, a metal oxide adsorbent, is hydrated in a humid environment to
457 generate a surface charge, and the interaction between F^- and metal oxides at low pH was
458 modeled assuming the following ligand exchange reaction (Tripathy et al. 2006).
459

$$MOH + H^+ \leftrightarrow MOH_2^+ \quad (10)$$

$$MOH_2 + F^- \leftrightarrow MF + H_2O \quad (11)$$

460
461 M represents a metal ion (here, Al).
462 Fluoride adsorption by Al-KNF-300 was studied in a pH range of 3–11, as shown in Fig. 5.
463 Fluoride adsorption decreased with increasing pH, possibly because of competition between
464 F^- and OH^- on the adsorbent surface (Babaeivelni and Khodadoust 2013). In addition, at an
465 acidic pH, some F^- can combine with H^+ to form hydrogen fluoride (He et al. 2019). Therefore,
466 a solution pH as low as 3 is effective for fluoride adsorption by Al-KNF-300.
467 Various anions are typically present in polluted water and can affect fluoride adsorption by
468 Al-KNF-300 because they compete with F^- at the active sites on the adsorbent surface.
469 Therefore, adsorption experiments were performed in the presence of HCO_3^-, SO_4^{2-}, Cl^-, and
470 NO_3^-, which can compete with fluoride. Each anion was added to the fluoride solution at a

concentration of 1 mM or 10 mM to react with the adsorbent; the results are shown in Fig. 6. The magnitude of the negative effects on fluoride adsorption is ordered as follows: HCO_3^- > SO_4^{2-} > NO_3^- > Cl^-. This order may be related to the ratio of charges to radii of the anions (Dhillon et al. 2017). Cl^- and NO_3^- form a surface complex consisting of an outer sphere, whereas sulfate forms a surface complex consisting of outer and inner spheres (Tang et al. 2009b). Therefore, Cl^- and NO_3^- have less effect on fluoride adsorption than SO_4^{2-}. HCO_3^- has the most significant effect on fluoride removal. The reason is that HCO_3^- is hydrolyzed in aqueous solution, increasing the solution pH, and the alkalization of this solution hinders the adsorption of fluoride (Onyango et al. 2004).

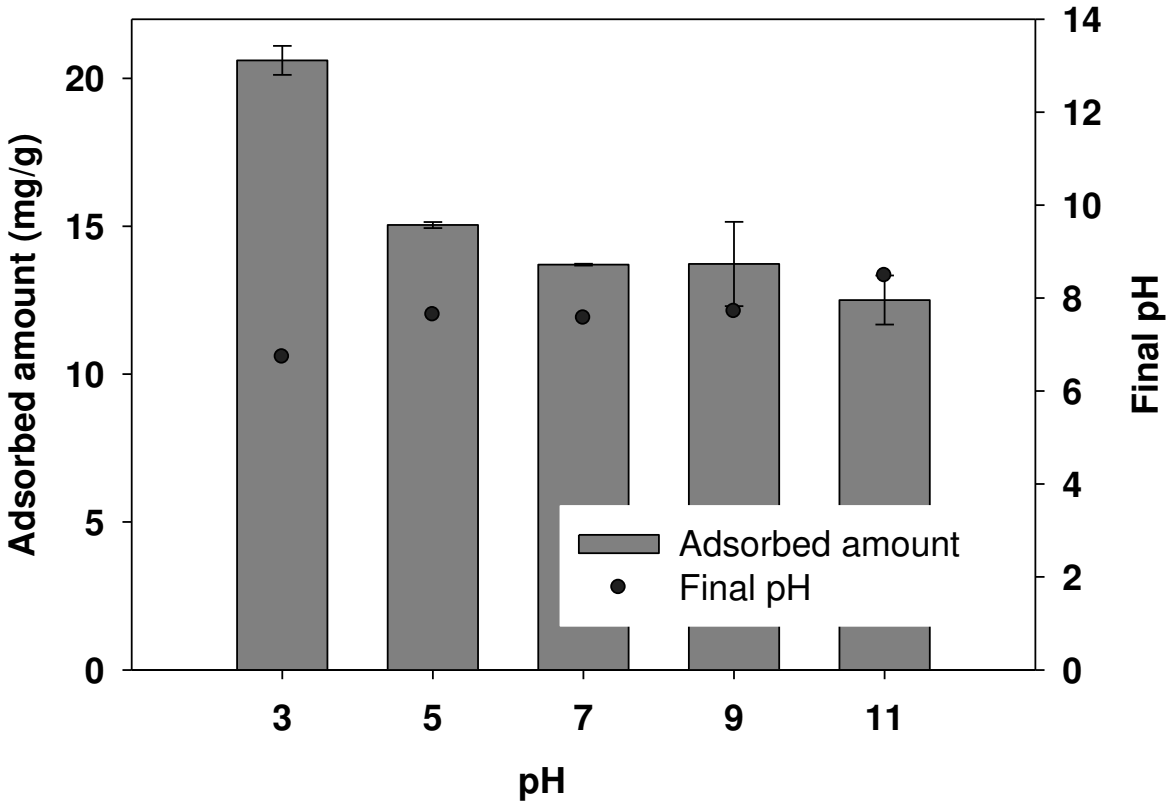

481

482 **Fig. 5.** Effect of solution pH on fluoride adsorption by Al-KNF-300 (initial F concentration:

483 100 mg/L, adsorbent dose: 3.33 g/L, reaction temperature: 25 °C, time: 12 h)

484

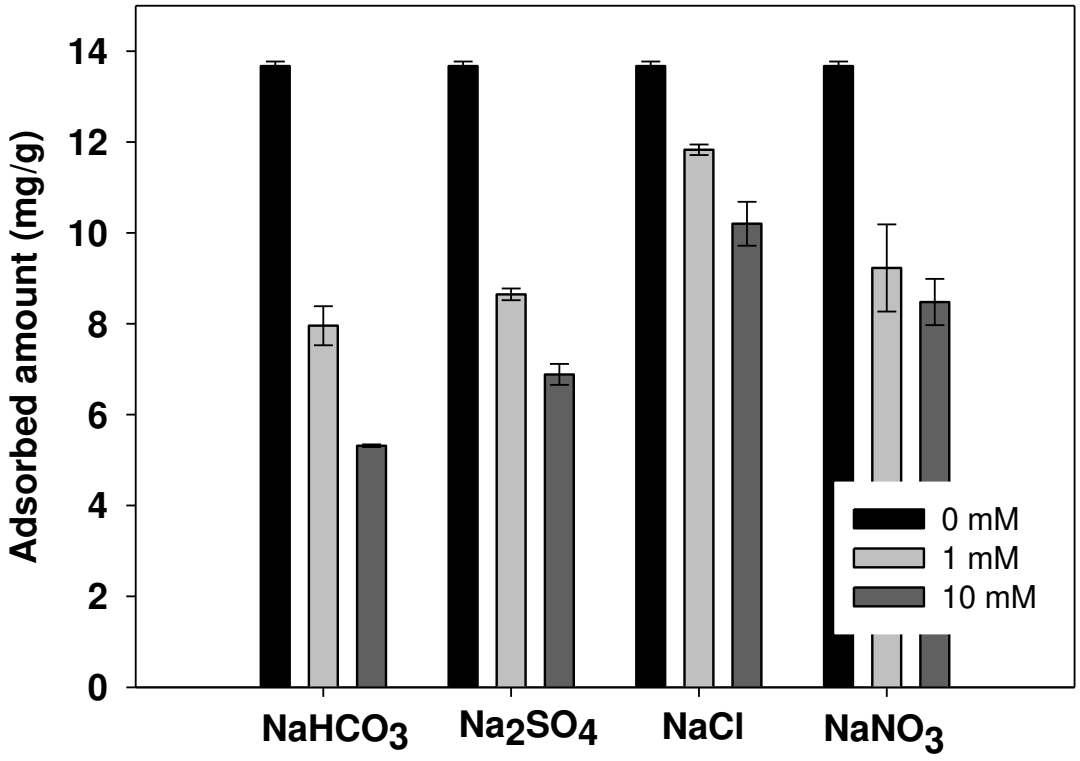

Fig. 6. Effect of the presence of anions on fluoride adsorption by Al-KNF-300 (initial F concentration: 100 mg/L, adsorbent dose: 3.33 g/L, reaction temperature: 25 °C, time: 12 h)

3.6 Effect of adsorbent dose on adsorption ratio and adsorption capacity

The effect of adsorbent dose on fluoride removal was examined using a fluoride concentration of 100 mg/L and various adsorbent doses (3.33–16.67 g/L). The results are shown in Fig. S5. As the adsorbent dose was increased from 3.33 to 16.67 g/L, the fluoride removal efficiency increased from 40.65% to 99.23%. The reason is that the number of active surface sites for fluoride adsorption increased with increasing adsorbent dose (Salifu et al. 2013). The fluoride adsorption per unit mass of adsorbent decreased as the adsorbent dose increased. The reason is that the adsorption potential of fluoride per unit mass decreases with increasing adsorbent dose (Wang et al. 2009). At lower adsorbent doses, all sites are fully exposed to fluoride adsorption, and the surface saturates more quickly; consequently, q_e

499 increases. By contrast, at higher adsorbent doses, adsorption occurs selectively at lower-energy
500 sites, and q_e decreases (Biswas et al. 2009).

501 The maximum fluoride adsorption efficiency (%) of Al-KNF-300 obtained in this study
502 was compared with those of various other adsorbents (Table 3). Because direct comparison
503 with other adsorbents is difficult, the initial fluoride concentration and adsorbent capacity are
504 also shown. Al-KNF-300 had higher fluoride removal efficiency than other adsorbents reported
505 in the literature. In addition, the initial fluoride concentration, which can affect the adsorption
506 efficiency, was also higher than those in the literature, indicating that Al-KNF-300 can adsorb
507 sufficient fluoride even at a relatively high fluoride concentration. When a 100 mg/L fluoride
508 solution was treated with an adsorbent dose of 16.67 g/L, the residual fluoride concentration
509 was 0.84 mg/L, which is within the acceptable range for drinking water (<1.5 mg/L) (World
510 Health Organization 2017).

511

512 **Table 3.** Maximum fluoride adsorption efficiency (%) of Al-KNF-300 and various other
513 adsorbents

Adsorbent	Maximum adsorption efficiency (%)	Initial fluoride concentration (mg/L)	Dose (g/L)	Reference
Laterite	60	3	4	Iriel et al. (2018)
Protonated chitosan particles	72	20	2	Kusrini et al. (2015)
N-trimethylammonium-modified kenaf	77.50	20	1.2	Yusof et al. (2015)
Activated aluminum oxide	80	100	20	Dhawane et al. (2018)
Quicklime	80.60	50	5	Islam and Patel (2007)

Waste carbon slurry	88.20	100	3	Gupta et al. (2007)
Corn stover biochar	91.41	10	10	Mohan et al. (2014)
Al-modified food waste biochar	91.42	300	6.7	Meilani et al. (2021)
Amorphous aluminum hydroxide hollow spheres	94.13	20	1	Zhang et al. (2016)
Magnetic corn stover biochar	97.71	10	10	Mohan et al. (2014)
Al-modified kenaf biochar	99.23	100	16.67	This study

4. Conclusion

The stems of kenaf, a plant with high productivity and adsorption potential, were modified to produce Al-impregnated kenaf biochar (Al-KNF-BC) for use as a fluoride adsorbent. Al-KNF-BCs were produced at various pyrolysis temperatures; Al-KNF-300, which was produced at 300 °C, was the most effective adsorbent for fluoride removal. Al-KNF-300 has more pores and a lower Cl content than the material without heat treatment. Amorphous Al was present on Al-KNF-300, whereas Al_2O_3 was present on the other Al-KNF-BCs; the presence of amorphous Al contributed to the high fluoride adsorption capacity of Al-KNF-300. Fluoride adsorption by Al-KNF-300 reached equilibrium at 12 h, and chemisorption is the limiting step in fluoride adsorption by Al-KNF-300. The Langmuir model was found to be most suitable for modeling fluoride adsorption by Al-KNF-300, indicating that adsorption occurred in a monolayer on a homogeneous surface. The adsorbed amount per unit mass of Al-KNF-300 at equilibrium was 14.22 mg/g, which is comparable to those of previously reported adsorbents. At an adsorbent dose of 3.33 g/L, Al-KNF-300 reduced the fluoride concentration of 5–30 mg/L fluoride solutions to the acceptable drinking water standard (<1.5 mg/L). Thermodynamic adsorption experiments showed that adsorption is an endothermic reaction that increases the randomness. Low pH is favorable for fluoride adsorption by Al-KNF-300

because the adsorbent has a positive surface charge, and there is less competition with OH^- at low pH. The effect of anion competition on fluoride adsorption by Al-KNF-300 followed the order $HCO_3^- > SO_4^{2-} > NO_3^- > Cl^-$. With increasing adsorbent capacity, the fluoride adsorption efficiency increased to 99.23%, but the fluoride adsorption amount per unit mass of adsorbent decreased. Al-KNF-300 is an inexpensive, value-added product that can remove fluoride from fluoride-contaminated water and bring the fluoride concentration to the drinking water standard.

REFERENCE

Abdel-Fattah TM, Mahmoud ME, Ahmed SB, Huff MD, Lee JW, Kumar S (2015) Biochar from woody biomass for removing metal contaminants and carbon sequestration. J Ind Eng Chem 22:103-109. https://doi.org/10.1016/j.jiec.2014.06.030

Abdilla RM, Rasrendra CB, Heeres HJ (2018) Kinetic studies on the conversion of levoglucosan to glucose in water using Brønsted acids as the catalysts. Ind Eng Chem Res 57.9:3204-3214. https://doi.org/10.1021/acs.iecr.8b00013

Ahamad KU, Singh R, Baruah I, Choudhury H, Sharma MR (2018) Equilibrium and kinetics modeling of fluoride adsorption onto activated alumina, alum and brick powder. Groundw Sustain Dev 7:452-458. https://doi.org/10.1016/j.gsd.2018.06.005

Ahmed MB, Zhou JL, Ngo HH, Guo W, Chen M (2016) Progress in the preparation and application of modified biochar for improved contaminant removal from water and wastewater. Bioresour Technol 214:836-851. https://doi.org/10.1016/j.biortech.2016.05.057

Amini M, Mueller KIM, Abbaspour KC, Rosenberg T, Afyuni M, Møller KN, Johnson CA (2008) Statistical modeling of global geogenic fluoride contamination in groundwaters. Environ Sci Technol 42.10:3662-3668. https://doi.org/10.1021/es071958y

556 Amor Z, Bariou B, Mameri N, Taky M, Nicolas S, Elmidaoui A (2001) Fluoride removal
557 from brackish water by electrodialysis. Desalination 133.3:215-223.
558 https://doi.org/10.1016/S0011-9164(01)00102-3
559 Azwa ZN, Yousif BF (2013) Characteristics of kenaf fibre/epoxy composites subjected to
560 thermal degradation. Polym Degrad Stab 98.12:2752-2759.
561 https://doi.org/10.1016/j.polymdegradstab.2013.10.008
562 Babaeivelni K, Khodadoust AP (2013) Adsorption of fluoride onto crystalline titanium
563 dioxide: Effect of pH, ionic strength, and co-existing ions. J Colloid Interface Sci
564 394:419-427. https://doi.org/10.1016/j.jcis.2012.11.063
565 Biswas K, Bandhoyapadhyay D, Ghosh UC (2007) Adsorption kinetics of fluoride on iron
566 (III)-zirconium (IV) hybrid oxide. Adsorption 13.1:83-94.
567 https://doi.org/10.1007/s10450-007-9000-1
568 Biswas K, Gupta K, Ghosh UC (2009) Adsorption of fluoride by hydrous iron (III)–tin (IV)
569 bimetal mixed oxide from the aqueous solutions. Chem Eng Sci, 149.1-3:196-206.
570 https://doi.org/10.1016/j.cej.2008.09.047
571 Borna MO, Pirsaheb M, Niri MV, Mashizie RK, Kakavandi B, Zare MR, Asadi A (2016)
572 Batch and column studies for the adsorption of chromium (VI) on low-cost Hibiscus
573 Cannabinus kenaf, a green adsorbent. J Taiwan Inst Chem Eng, 68:80-89.
574 https://doi.org/10.1016/j.jtice.2016.09.022
575 Çengeloğlu Y, Kır E, Ersöz M (2002) Removal of fluoride from aqueous solution by using
576 red mud. Sep Purif Technol 28.1:81-86. https://doi.org/10.1016/S1383-
577 5866(02)00016-3

578 Cengeloglu Y, Tor A, Ersoz M, Arslan G (2006) Removal of nitrate from aqueous solution by
579 using red mud. Sep Purif Technol 51.3:374-378.
580 https://doi.org/10.1016/j.seppur.2006.02.020
581 Chaari I, Fakhfakh E, Medhioub M, Jamoussi F (2019) Comparative study on adsorption of
582 cationic and anionic dyes by smectite rich natural clays. J Mol Struct 1179:672-677.
583 https://doi.org/10.1016/j.molstruc.2018.11.039
584 Chang MF, Liu JC (2007) Precipitation removal of fluoride from semiconductor wastewater.
585 J Environ Eng, 133.4:419-425. http:// doi.org/10.1061/(ASCE)0733-
586 9372(2007)133:4(419)
587 Chen GJ, Peng CY, Fang JY, Dong YY, Zhu XH, Cai HM (2016) Biosorption of fluoride from
588 drinking water using spent mushroom compost biochar coated with aluminum
589 hydroxide. Desalination Water Treat 57.26:12385-12395.
590 https://doi.org/10.1080/19443994.2015.1049959
591 Chen J, Yang R, Zhang Z, Wu D (2022) Removal of fluoride from water using aluminum
592 hydroxide-loaded zeolite synthesized from coal fly ash. J Hazard Mater 421:126817.
593 https://doi.org/10.1016/j.jhazmat.2021.126817
594 Chen N, Zhang Z, Feng C, Li M, Chen R, Sugiura N (2011) Investigations on the batch and
595 fixed-bed column performance of fluoride adsorption by Kanuma mud. Desalination
596 268.1-3:76-82. https://doi.org/10.1016/j.desal.2010.09.053
597 Chen N, Zhang Z, Feng C, Sugiura, N, Li M, Chen R (2010) Fluoride removal from water by
598 granular ceramic adsorption. J Colloid Interface Sci 348.2:579-584.
599 https://doi.org/10.1016/j.jcis.2010.04.048
600 Cho EJ, Kang JK, Moon JK, Um BH, Lee CG, Jeong S, Park SJ (2021) Removal of triclosan
601 from aqueous solution via adsorption by kenaf-derived biochar: Its adsorption

602 mechanism study via spectroscopic and experimental approaches. J Environ Chem Eng
603 9.6 106343. https://doi.org/10.1016/j.jece.2021.106343
604 Choi MY, Lee JI, Lee CG, Park SJ (2021) Feasibility of using calcined Patinopecten
605 yessoensis shells for fluoride removal and investigation of the fluoride removal
606 mechanism. Desalination Water Treat 233:292-302.
607 https://doi.org/10.5004/dwt.2021.27551
608 Das N, Pattanaik P, Das R (2005) Defluoridation of drinking water using activated titanium
609 rich bauxite. J Colloid Interface Sci 292.1:1-10.
610 https://doi.org/10.1016/j.jcis.2005.06.045
611 Dhawane SH, Khan AA, Singh K, Tripathi A, Hasda, R, Halder G (2018) Insight into
612 Optimization, isotherm, kinetics, and thermodynamics of fluoride adsorption onto
613 activated alumina. Environ Prog Sustain Energy, 37.2:766-776.
614 https://doi.org/10.1002/ep.12814
615 Dhillon A, Soni SK, Kumar D (2017) Enhanced fluoride removal performance by Ce–Zn
616 binary metal oxide: adsorption characteristics and mechanism. J Fluor Chem 199:67-76.
617 https://doi.org/10.1016/j.jfluchem.2017.05.002
618 Ding Z, Xu X, Phan T, Hu X, Nie, G (2018) High adsorption performance for As (III) and As
619 (V) onto novel aluminum-enriched biochar derived from abandoned Tetra Paks.
620 Chemosphere 208:800-807. https://doi.org/10.1016/j.chemosphere.2018.06.050
621 Nascimento DC, Silva MGC, Vieira MGA (2021) Adsorption of propranolol hydrochloride
622 from aqueous solutions onto thermally treated bentonite clay: A complete batch system
623 evaluation. J Mol Liq 337:116442. https://doi.org/10.1016/j.molliq.2021.116442
624 Ebadi M, Buskaran K, Bullo S, Hussein MZ, Fakurazi S, Pastorin G (2021) Drug delivery
625 system based on magnetic iron oxide nanoparticles coated with (polyvinyl alcohol-

626 zinc/aluminium-layered double hydroxide-sorafenib). Alex Eng J 60.1:733-747.
627 https://doi.org/10.1016/j.aej.2020.09.061
628 Elazhar F, Tahaikt M, Achatei A et al (2009) Economical evaluation of the fluoride removal
629 by nanofiltration. Desalination 249.1:154-157.
630 https://doi.org/10.1016/j.desal.2009.06.017
631 Fan C, Yin N, Cai X et al (2021) Stabilization of fluorine-contaminated soil in aluminum
632 smelting site with biochar loaded iron-lanthanide and aluminum-lanthanide bimetallic
633 materials. J Hazard. Mater 426:128072. https://doi.org/10.1016/j.jhazmat.2021.128072
634 Fan X, Parker DJ, Smith MD (2003) Adsorption kinetics of fluoride on low cost materials.
635 Water Res 37.20:4929-4937. https://doi.org/10.1016/j.watres.2003.08.014
636 Farooqi A, Masuda H, Firdous N (2007) Toxic fluoride and arsenic contaminated
637 groundwater in the Lahore and Kasur districts, Punjab, Pakistan and possible
638 contaminant sources. Environ Pollut 1453:839-849.
639 https://doi.org/10.1016/j.envpol.2006.05.007
640 Farrah H, Slavek J, Pickering WF (1987) Fluoride interactions with hydrous aluminum
641 oxides and alumina. Soil Res 25.1:55-69. https://doi.org/10.1071/SR9870055
642 Feng N, Guo X, Liang S, Zhu Y, Liu J (2011) Biosorption of heavy metals from aqueous
643 solutions by chemically modified orange peel. J Hazard Mater 185.1:49-54.
644 https://doi.org/10.1016/j.jhazmat.2010.08.114
645 Ferrara F, Orsini A, Plaisant A, Pettinau A (2014) Pyrolysis of coal, biomass and their blends:
646 Performance assessment by thermogravimetric analysis. Bioresour Technol 171:433-
647 441. https://doi.org/10.1016/j.biortech.2014.08.104
648 Freundlich H (1907) Über die adsorption in lösungen. Z Phys Chem,57.1:385-470.
649 https://doi.org/10.1515/zpch-1907-5723

650 Ghorai S, Pant KK (2004) Investigations on the column performance of fluoride adsorption
651 by activated alumina in a fixed-bed. Chem Eng J 98.1-2:165-173.
652 https://doi.org/10.1016/j.cej.2003.07.003
653 Gong WX, Qu JH, Liu RP, Lan HC (2012) Adsorption of fluoride onto different types of
654 aluminas. Chem Eng J 189:126-133. https://doi.org/10.1016/j.cej.2003.07.003
655 Guo Y, Rockstraw DA (2006) Physical and chemical properties of carbons synthesized from
656 xylan, cellulose, and Kraft lignin by H_3PO_4 activation. Carbon 44.8:1464-1475.
657 https://doi.org/10.1016/j.carbon.2005.12.002
658 Gupta VK, Ali I, Saini VK (2007) Defluoridation of wastewaters using waste carbon slurry.
659 Water Res. 41.15:3307-3316. https://doi.org/10.1016/j.watres.2007.04.029
660 Ha ES, Ha DH, Kuk DH et al (2017) Solubility of cilostazol in the presence of polyethylene
661 glycol 4000, polyethylene glycol 6000, polyvinylpyrrolidone K30, and poly (1-
662 vinylpyrrolidone-co-vinyl acetate) at different temperatures. J Chem Thermodyn 113:6-
663 10. https://doi.org/10.1016/j.jct.2017.05.040
664 Harrington LF, Cooper EM, Vasudevan D (2003) Fluoride sorption and associated aluminum
665 release in variable charge soils. J Colloid Interface Sci 267.2:302-313.
666 https://doi.org/10.1016/S0021-9797(03)00609-X
667 Hasfalina CM, Maryam RZ, Luqman CA, Rashid M (2010) The potential use of kenaf as a
668 bioadsorbent for the removal of copper and nickel from single and binary aqueous
669 solution. J Nat Fibers 7.4:267-275. https://doi.org/10.1080/15440478.2010.527508
670 Hasfalina CM, Maryam RZ, Luqman CA, Rashid M (2012) Adsorption of copper (II) from
671 aqueous medium in fixed-bed column by kenaf fibres. APCBEE procedia 3:255-263.
672 https://doi.org/10.1016/j.apcbee.2012.06.079

673 He Y, Zhang L, An X, Wan G, Zhu W, Luo Y (2019) Enhanced fluoride removal from water
674 by rare earth (La and Ce) modified alumina: Adsorption isotherms, kinetics,
675 thermodynamics and mechanism. Sci Total Environ 688:184-198.
676 https://doi.org/10.1016/j.scitotenv.2019.06.175
677 Ho YS, McKay G (1998) Kinetic model for lead (II) sorption on to peat. Adsorpt Sci Technol
678 16.4:243-255. https://doi.org/10.1177/026361749801600401
679 Iriel A, Bruneel SP, Schenone N, Cirelli AF (2018) The removal of fluoride from aqueous
680 solution by a lateritic soil adsorption: kinetic and equilibrium studies. Ecotoxicol
681 Environ Saf 149:166-172. https://doi.org/10.1016/j.ecoenv.2017.11.016
682 Islam M, Patel RK (2007) Evaluation of removal efficiency of fluoride from aqueous solution
683 using quick lime. J Hazard Mater, 143.1-2:303-310.
684 https://doi.org/10.1016/j.jhazmat.2006.09.030
685 Jagtap S, Yenkie MKN, Labhsetwar N, Rayalu S (2011) Defluoridation of drinking water
686 using chitosan based mesoporous alumina. Microporous Mesoporous Mater 142.2-
687 3:454-463. https://doi.org/10.1016/j.micromeso.2010.12.028
688 Jones S, Burt BA, Petersen PE, Lennon MA (2005) The effective use of fluorides in public
689 health. World Health Organ 83:670-676. https://doi.org/10.1590/S0042-
690 96862005000900012.
691 Karthikeyan G, Pius A, Alugumuthu G (2005) Fluoride adsorption studies of montmorillonite
692 clay. Indian J Chem Tech 12:263–272. http://nopr.niscair.res.in/handle/123456789/8640
693 Kasperiski FM, Lima EC, Umpierres CS et al (2018) Production of porous activated carbons
694 from Caesalpinia ferrea seed pod wastes: highly efficient removal of captopril from
695 aqueous solutions. J Clean Prod197:919-929.
696 https://doi.org/10.1016/j.jclepro.2018.06.146

697 Khan TA, Khan EA (2015) Removal of basic dyes from aqueous solution by adsorption onto
698 binary iron-manganese oxide coated kaolinite: non-linear isotherm and kinetics
699 modeling. Appl. Clay Sci 107:70-77. https://doi.org/10.1016/j.clay.2015.01.005
700 Kim SJ, Um BH (2020). Process variable optimization of kenaf two-stage fractionation based
701 on dilute hydrochloric acid followed by ethanol organosolv for component separation.
702 Bioenergy Res 13.1:249-259. https://doi.org/10.1007/s12155-019-10057-y
703 Kusrini E, Sofyan N, Suwartha N, Yesya G, Priadi CR (2015) Chitosan-praseodymium
704 complex for adsorption of fluoride ions from water. J Rare Earths 33.10:1104-1113.
705 https://doi.org/10.1016/S1002-0721(14)60533-0
706 Lagergren SK (1898) About the theory of so-called adsorption of soluble substances. Sven
707 Vetenskapsakad Handingarl 24:1-39.
708 Langmuir I (1916) The constitution and fundamental properties of solids and liquids. Part I.
709 Solids. J Am Chem Soc 38.11:2221-2295. https://doi.org/10.1021/ja02268a002
710 Lee G, Chen C, Yang ST, Ahn WS (2010) Enhanced adsorptive removal of fluoride using
711 mesoporous alumina. Microporous Mesoporous Mater 127.1-2:152-156.
712 https://doi.org/10.1016/j.micromeso.2009.07.007
713 Lee JI, Hong SH, Lee CG, Park SJ (2021a) Fluoride removal by thermally treated egg shells
714 with high adsorption capacity, low cost, and easy acquisition. Environ Sci Pollut Res
715 28.27: 35887-35901. https://doi.org/10.1007/s11356-021-13284-z
716 Lee JI, Kang JK, Hong SH, Lee CG, Jeong S, Park SJ (2021b) Thermally treated Mytilus
717 coruscus shells for fluoride removal and their adsorption mechanism. Chemosphere
718 263:128328. https://doi.org/10.1016/j.chemosphere.2020.128328

719 Leyva-Ramos R, Rivera-Utrilla J, Medellin-Castillo NA, Sanchez-Polo M (2010) Kinetic
720 modeling of fluoride adsorption from aqueous solution onto bone char. Chem Eng J
721 158.3:458-467. https://doi.org/10.1016/j.cej.2010.01.019
722 Li YH, Wang S, Cao A et al (2001) Adsorption of fluoride from water by amorphous alumina
723 supported on carbon nanotubes. Chem Phys Lett 350.5-6:412-416.
724 https://doi.org/10.1016/S0009-2614(01)01351-3
725 Lin B, Zhou J, Qin Q, Song X, Luo Z (2019) Thermal behavior and gas evolution
726 characteristics during co-pyrolysis of lignocellulosic biomass and coal: A TG-FTIR
727 investigation. J Anal Appl Pyrolysis 144:104718.
728 https://doi.org/10.1016/j.jaap.2019.104718
729 Mahfoudhi N, Boufi S (2020) Porous material from cellulose nanofibrils coated with
730 aluminum hydroxyde as an effective adsorbent for fluoride. J Environ Chem Eng,
731 8.3:103779. https://doi.org/10.1016/j.jece.2020.103779
732 Mahmoud DK, Salleh MAM, Karim WAWA et al (2012) Batch adsorption of basic dye using
733 acid treated kenaf fibre char: equilibrium, kinetic and thermodynamic studies. Chem
734 Eng J 181:449-457. https://doi.org/10.1016/j.cej.2011.11.116
735 Malik DS, Jain CK, Yadav AK (2017) Removal of heavy metals from emerging cellulosic
736 low-cost adsorbents: a review. Appl Water Sci 7.5:2113-2136.
737 https://doi.org/10.1007/s13201-016-0401-8
738 Mayakaduwa SS, Kumarathilaka P, Herath I et al (2016) Equilibrium and kinetic mechanisms
739 of woody biochar on aqueous glyphosate removal. Chemosphere 144:2516-2521.
740 https://doi.org/10.1016/j.chemosphere.2015.07.080

741 Medellin-Castillo NA, Leyva-Ramos R, Ocampo-Perez R et al (2007). Adsorption of fluoride
742 from water solution on bone char. Ind. Eng. Chem 46.26:9205-9212.
743 https://doi.org/10.1021/ie070023n
744 Meilani V, Lee JI, Kang JK, Lee CG, Jeong S, Park SJ (2021) Application of aluminum-
745 modified food waste biochar as adsorbent of fluoride in aqueous solutions and
746 optimization of production using response surface methodology. Microporous
747 Mesoporous Mater 312:110764. https://doi.org/10.1016/j.micromeso.2020.110764
748 Mian MM, Liu G (2018) Recent progress in biochar-supported photocatalysts: synthesis, role
749 of biochar, and applications. RSC Adv 8.26:14237-14248.
750 https://doi.org/10.1039/C8RA02258E
751 Mirsoleimani-azizi SM, Setoodeh P, Zeinali S, Rahimpour MR (2018) Tetracycline antibiotic
752 removal from aqueous solutions by MOF-5: Adsorption isotherm, kinetic and
753 thermodynamic studies. J Environ Chem Eng 6.5:6118-6130.
754 https://doi.org/10.1016/j.jece.2018.09.017
755 Mohan D, Kumar S, Srivastava A (2014) Fluoride removal from ground water using magnetic
756 and nonmagnetic corn stover biochars. Ecol Eng 73:798-808.
757 https://doi.org/10.1016/j.ecoleng.2014.08.017
758 Nishino T, Hirao K, Kotera M, Nakamae K, Inagaki H (2003) Kenaf reinforced
759 biodegradable composite. Compos Sci Technol 63.9:1281-1286.
760 https://doi.org/10.1016/S0266-3538(03)00099-X
761 Onyango MS, Kojima Y, Aoyi O, Bernardo EC, Matsuda H (2004) Adsorption equilibrium
762 modeling and solution chemistry dependence of fluoride removal from water by
763 trivalent-cation-exchanged zeolite F-9. J Colloid Interface Sci 279.2:341-350.
764 https://doi.org/10.1016/j.jcis.2004.06.038

765 Podgorny PC, McLaren L (2015) Public perceptions and scientific evidence for perceived
766 harms/risks of community water fluoridation: an examination of online comments
767 pertaining to fluoridation cessation in Calgary in 2011. Can J Public Health 106.6:e413-
768 e425. https://doi.org/10.17269/CJPH.106.5031
769 Rahman ML, Biswas TK, Sarkar SM, Yusoff MM, Sarjadi MS, Arshad SE, Musta B (2017)
770 Adsorption of rare earth metals from water using a kenaf cellulose-based poly
771 (hydroxamic acid) ligand. J Mol Liq 243:616-623.
772 https://doi.org/10.1016/j.molliq.2017.08.096
773 Ramos-Vargas S, Alfaro-Cuevas-Villanueva R, Huirache-Acuña R, Cortés-Martínez R (2018)
774 Removal of fluoride and arsenate from aqueous solutions by aluminum-modified guava
775 seeds. Appl Sci, 8.10:1807. https://doi.org/10.3390/app8101807
776 Rapacz-Kmita A, Paluszkiewicz C, Ślósarczyk A, Paszkiewicz Z (2005) FTIR and XRD
777 investigations on the thermal stability of hydroxyapatite during hot pressing and
778 pressureless sintering processes. J Mol Struct 744:653-656.
779 https://doi.org/10.1016/j.molstruc.2004.11.070
780 Rojas-Mayorga CK, Bonilla-Petriciolet A, Silvestre-Albero J, Aguayo-Villarreal IA,
781 Mendoza-Castillo DI (2015) Physico-chemical characterization of metal-doped bone
782 chars and their adsorption behavior for water defluoridation. Appl Surf Sci 355:748-760.
783 https://doi.org/10.1016/j.apsusc.2015.07.163
784 Roy S, Sengupta S, Manna S, Das P (2018) Chemically reduced tea waste biochar and its
785 application in treatment of fluoride containing wastewater: Batch and optimization using
786 response surface methodology. Process Saf Environ Prot 116:553-563.
787 https://doi.org/10.1016/j.psep.2018.03.009

788 Salifu A, Petrusevski B, Ghebremichael K, Modestus L, Buamah R, Aubry C, Amy GL
789 (2013) Aluminum (hydr) oxide coated pumice for fluoride removal from drinking water:
790 Synthesis, equilibrium, kinetics and mechanism. Chem Eng J 228:63-74.
791 https://doi.org/10.1016/j.cej.2013.04.075
792 Samadi MT, Zarrabi M, Sepehr MN, Ramhormozi SM, Azizian S, Amrane A (2014) Removal
793 of fluoride ions by ion exchange resin: kinetic and equilibrium studies. Eng Manag J
794 13.1. http://omicron.ch.tuiasi.ro/EEMJ/
795 Sellers T (1999) Kenaf properties, processing and products. Mississippi State University,
796 Skudai
797 Shahmoradi AR, Talebibahmanbigloo N, Javidparvar AA, Bahlakeh G, Ramezanzadeh B
798 (2020) Studying the adsorption/inhibition impact of the cellulose and lignin compounds
799 extracted from agricultural waste on the mild steel corrosion in HCl solution. J Mol Liq
800 304:112751. https://doi.org/10.1016/j.molliq.2020.112751
801 Shamsuddin MS, Yusoff NRN, Sulaiman MA (2016) Synthesis and characterization of
802 activated carbon produced from kenaf core fiber using H_3PO_4 activation. Procedia Chem
803 19:558-565. https://doi.org/10.1016/j.proche.2016.03.053
804 Stefaniuk M, Oleszczuk P (2015) Characterization of biochars produced from residues from
805 biogas production. J Anal Appl Pyrolysis 115:157-165.
806 https://doi.org/10.1016/j.jaap.2015.07.011
807 Sun Y, Fang Q, Dong J, Cheng X, Xu J (2011) Removal of fluoride from drinking water by
808 natural stilbite zeolite modified with Fe (III). Desalination 277.1-3:121-127.
809 https://doi.org/10.1016/j.desal.2011.04.013

Sun ZX, Zheng TT, Bo QB, Du M, Forsling W (2008) Effects of calcination temperature on the pore size and wall crystalline structure of mesoporous alumina. J Colloid Interface Sci 319.1:247-251. https://doi.org/10.1016/j.jcis.2007.11.023

Tang Y, Guan X, Su T, Gao N, Wang J (2009a) Fluoride adsorption onto activated alumina: Modeling the effects of pH and some competing ions. Colloids Surf A Physicochem Eng 337.1-3:33-38. https://doi.org/10.1016/j.colsurfa.2008.11.027

Tang Y, Guan X, Wang J, Gao N, McPhail MR, Chusuei CC (2009b) Fluoride adsorption onto granular ferric hydroxide: effects of ionic strength, pH, surface loading, and major co-existing anions. J Hazard Mater 171.1-3:774-779. https://doi.org/10.1016/j.jhazmat.2009.06.079

Tchomgui-Kamga E, Alonzo V, Nanseu-Njiki CP, Audebrand N, Ngameni E, Darchen A (2010) Preparation and characterization of charcoals that contain dispersed aluminum oxide as adsorbents for removal of fluoride from drinking water. Carbon 48.2:333-343. https://doi.org/10.1016/j.carbon.2009.09.034

Thue PS, Adebayo MA, Lima EC et al (2016). Preparation, characterization and application of microwave-assisted activated carbons from wood chips for removal of phenol from aqueous solution. J Mol Liq 223:1067-1080. https://doi.org/10.1016/j.molliq.2016.09.032

Tripathy SS, Bersillon JL, Gopal K (2006) Removal of fluoride from drinking water by adsorption onto alum-impregnated activated alumina. Sep Purif Technol 50.3:310-317. https://doi.org/10.1016/j.seppur.2005.11.036

Turner BD, Binning P, Stipp SLS (2005) Fluoride removal by calcite: evidence for fluorite precipitation and surface adsorption. Environ Sci Technol 39.24:9561-9568.

US Environmental Protection Agency (2020) Drinking water treatability database: fluoride, Regulated drinking water contaminants https://www.epa.gov/ground-water-and-drinking-water/national-primary-drinking-water-regulations, Accessed 5 Mar 2020

Wang G, Zhang S, Yao P, Chen Y, Xu X, Li T, Gong G (2018) Removal of Pb (II) from aqueous solutions by Phytolacca americana L. biomass as a low cost biosorbent. Arab J Chem 11.1:99-110. https://doi.org/10.1016/j.arabjc.2015.06.011

Wang SG, Ma Y, Shi YJ, Gong WX (2009) Defluoridation performance and mechanism of nano-scale aluminum oxide hydroxide in aqueous solution. J Chem Technol Biotechnol 84.7:1043-1050. https://doi.org/10.1002/jctb.2131

Wang Y, Reardon EJ (2001) Activation and regeneration of a soil sorbent for defluoridation of drinking water. J Appl Geochem 16.5:531-539. https://doi.org/10.1016/S0883-2927(00)00050-0

World Health Organization (2017) World Health Organization, Guidelines for drinking-water quality. Fourth edition incorporating the first addendum. http://apps.who.int/iris/bitstream/10665/254637/1/9789241549950-eng.pdf?ua=1 (2017), Accessed 18 Jul 2019

Yusof SRM, Zahri NAM, Koay YS, Nourouzi MM, Chuah LA, Choong TSY (2015) Removal of fluoride using modified kenaf as adsorbent. J Eng Sci Technol 10.11.

Zhang G, Zhang Q, Sun K, Liu X, Zheng W, Zhao Y (2011) Sorption of simazine to corn straw biochars prepared at different pyrolytic temperatures. Environ Pollut 159.10:2594-2601. https://doi.org/10.1016/j.envpol.2011.06.012

Zhang Y, Lin X, Zhou Q, Luo X (2016) Fluoride adsorption from aqueous solution by magnetic core-shell Fe_3O_4 alginate-La particles fabricated via electro-coextrusion. Appl Surf Sci, 389:34-45. https://doi.org/10.1016/j.envpol.2011.06.012

857 Zhou N, Guo X, Ye C, Yan L et al (2021) Enhanced fluoride removal from drinking water in
858 wide pH range using La/Fe/Al oxides loaded rice straw biochar. Water Supply. 22.1:779-
859 794. https://doi.org/10.2166/ws.2021.232
860 Zhang H, Ruan Y, Feng Y et al (2019). Solvent-free hydrothermal synthesis of gamma-
861 aluminum oxide nanoparticles with selective adsorption of Congo red. J Colloid
862 Interface Sci 536:180-188. https://doi.org/10.1016/j.jcis.2018.10.054
863 Zhuang Z, Wang L, Tang J (2021) Efficient removal of volatile organic compound by ball-
864 milled biochars from different preparing conditions. J Hazard Mater 406:124676.
865 https://doi.org/10.1016/j.jhazmat.2020.124676
866

Supplementary Files

This is a list of supplementary files associated with this preprint. Click to download.

- AlKNFBCFluorideSupplementary.docx